MOLECULAR ONCOLOGY 10 (2016) 704–718

available at www.sciencedirect.com

ScienceDirect

www.elsevier.com/locate/molonc

Monitoring vascular normalization induced by antiangiogenic treatment with ^{18}F-fluoromisonidazole-PET

Elena Hernández-Agudo[a], *Tamara Mondejar*[a], *Maria Luisa Soto-Montenegro*[b,c], *Diego Megías*[d], *Silvana Mouron*[a], *Jesus Sanchez*[a], *Manuel Hidalgo*[e], *Pedro Pablo Lopez-Casas*[e], *Francisca Mulero*[f], *Manuel Desco*[b,c,g], *Miguel Quintela-Fandino*[a,*]

[a]*Breast Cancer Clinical Research Unit, CNIO – Spanish National Cancer Research Center, Melchor Fernandez Almagro, 3, Madrid, 28029, Spain*
[b]*Unidad de Medicina y Cirugía Experimental, Instituto de Investigación Sanitaria Gregorio Marañon, Doctor Esquerdo, 46, Madrid, 28007, Spain*
[c]*CIBER de Salud Mental, Monforte de Lemos 3-5, Pabellón 11, Madrid, 28029, Spain*
[d]*Confocal Microscopy Unit, CNIO – Spanish National Cancer Research Center, Melchor Fernandez Almagro, 3, Madrid, 28029, Spain*
[e]*Gastrointestinal Cancer Clinical Research Unit, CNIO – Spanish National Cancer Research Center, Melchor Fernandez Almagro, 3, Madrid, 28029, Spain*
[f]*Molecular Imaging Unit, CNIO – Spanish National Cancer Research Center, Melchor Fernandez Almagro, 3, Madrid, 28029, Spain*
[g]*Aerospace Engineering and Bioengineering Department, Universidad Carlos III, Avenida de la Universidad, 30. Leganés, Madrid, 28911, Spain*

ARTICLE INFO

Article history:
Received 13 October 2015
Received in revised form
24 November 2015
Accepted 10 December 2015
Available online 22 December 2015

Keywords:
Antiangiogenics
Vascular normalization
Biomarker
^{18}F-misonidazole-PET
Pancreatic cancer
Breast cancer

ABSTRACT

Background: Rationalization of antiangiogenics requires biomarkers. Vascular re-normalization is one widely accepted mechanism of action for this drug class. The interstitium of tumors with abnormal vasculature is hypoxic. We sought to track vascular normalization with ^{18}F-misonidazole ([18F]-FMISO, a probe that detects hypoxia) PET, in response to window-of-opportunity (WoO) treatment with the antiangiogenic dovitinib.
Methods: Two patient-derived pancreas xenografts (PDXs; Panc215 and Panc286) and the spontaneous breast cancer model MMTV-PyMT were used. Animals were treated during 1 week of WoO treatment with vehicle or dovitinib, preceded and followed by [18F]-FMISO-PET, [18F]-FDG-PET, and histologic assessment (dextran extravasation, hypoxia and microvessel staining, and necrosis, cleaved caspase-3 and Ki67 measurements). After WoO treatment, gemcitabine (pancreas)/adriamycin (breast) or vehicle was added and animals were treated until the humane endpoint. Tumor growth inhibition (TGI) and survival were the parameters studied.
Results: [18F]-FMISO SUV did not change after dovitinib-WoO treatment compared to vehicle-WoO (0.54 vs. 0.6) treatment in Panc215, but it decreased significantly in Panc286 (0.58 vs. 1.18; $P < 0.05$). In parallel, 10-KDa perivascular dextran extravasation was not reduced with dovitinib or vehicle-WoO treatment in Panc215, but it was reduced in Panc286. Whereas the addition of dovitinib to gemcitabine was indifferent in Panc215, it

* *Corresponding author*. Breast Cancer Clinical Research Unit, CNIO – Spanish National Cancer Research Center, Melchor Fernández Almagro, 3, 28041, Madrid, Spain. Tel.: +34 917 328 000x2930; fax: +34 912 246 931.
E-mail address: mquintela@cnio.es (M. Quintela-Fandino).
http://dx.doi.org/10.1016/j.molonc.2015.12.011

increased TGI in Panc286 (TGI switched from −59% to +49%). [18F]-FMISO SUV changes were accompanied by an almost 100% increase in interstitial gemcitabine delivery (665–1260 ng/mL). The results were validated in the PyMT model.
Conclusions: [18F]-FMISO accurately monitored vascular re-normalization and improved interstitial chemotherapy delivery.

1. Introduction

Antiangiogenic agents are the most widely used biologic agents for routine care in oncology. Positive randomized phase III trials have led to FDA approval of different antiangiogenics in most epithelial malignancies. However, for those malignancies for which the drug class is approved and for those for which the results are not yet conclusive, there is room for improvement, especially regarding development of biomarker and/or predictive factors to rationalize therapeutic resources.

The precise mechanism of action for this drug class is not completely understood. The concept of antiangiogenesis has evolved much since Folkman's hypothesis (Folkman, 1971) which proposed that tumors would not be able to grow beyond ~0.1 mm if the development of novel blood vessels was abrogated. Novel antiangiogenics inhibit several proangiogenic factors, as opposed to the VEGF-specific agent bevacizumab. However, tumors still escape and develop resistance to novel, multi-targeted agents (Limaverde-Sousa et al., 2014). Active preclinical research has discovered more than a dozen factors and receptors involved in angiogenesis that can interact in hundreds of different potential ways due to the multi-specificity of receptors and factors, triggering a plethora of downstream physiopathologic effects (Lawler and Lawler, 2012; Petrillo et al., 2012; Richey and Hutson, 2013; Sakurai and Kudo, 2011; Yan et al., 2014). This high number of factors/receptors makes complete pharmacologic angiogenesis inhibition unrealistic. However, during the discovery of the complex temporal and spatial regulation of the angiogenesis process, one of the most relevant hypotheses regarding the mechanism of action of this drug class—vascular normalization—was developed (Jain, 2005, 2013b): the equilibrium between proangiogenic and antiangiogenic factors that maintain vessel homeostasis in normal tissues is deranged in cancer. This equilibrium has to be maintained within tight limits to generate normal blood vessels (Jain, 2005, 2013b; Kerbel, 2006). The disruption of the equilibrium in the tumor microenvironment leads to abnormal vessels. Abnormal tumor vessels are highly fenestrated, tortuous, and permeable; blood flow can be erratic, stagnant and/or retrograde instead of unidirectional and constant. Together with abnormal development and function of the drainage systems, these factors lead to increased interstitial pressure and intercellular matrix edema (Jain, 2013b). In addition, the maximum distance between vessels and cells is heterogeneous and variable (Hlatky et al., 2002; Jain, 2005, 2013b; Kerbel, 2006). Heterogeneous tumor cell subpopulations with different cell growth and metabolic rates have varying demands for oxygen and nutrients from the blood vessels (Hlatky et al., 2002). Thus, large areas of the tumor are poorly irrigated and hypoxic (Hlatky et al., 2002; Jain, 2005, 2013b; Kerbel, 2006). Hypoxia itself is a tumor progression factor (Gilkes et al., 2014). Vascular abnormality, characterized by impaired blood supply and interstitial hypertension, interferes with the delivery of (chemo) therapeutics to solid tumors (Jain, 2005, 2013b; Kerbel, 2006). This situation can be reached by an excess or by a deficit of proangiogenic or antiangiogenic factors in the tumor microenvironment (Jain, 2005, 2013b; Kerbel, 2006). According to this theory, when an antiangiogenic agent is administered, this abnormal balance could be restored to almost normal levels, and vasculature can be "re-normalized" (Jain, 2005, 2013b; Kerbel, 2006). Subsequently, chemotherapy delivery would be improved. The hypothesis is plausible because antiangiogenic agents alone have no effect on most epithelial malignancies (apart from non-liver, non-kidney cancers) (Cobleigh et al., 2003; Yang et al., 2003). However, when added to chemotherapy, the response rate is usually much higher than that reported for chemotherapy alone (Burger et al., 2011; Hurwitz et al., 2004; Miller et al., 2007; Perren et al., 2011; Sandler et al., 2006).

This hypothesis also has drawbacks. First, the duration of this normalization response is probably limited and could be followed by vascular pruning; an inadequate vascular network would interfere with chemotherapy delivery (Jain, 2005, 2013b; Kerbel, 2006). Second, some antiangiogenics have been demonstrated to normalize the vasculature and hypoxia, whereas others have been shown to induce the opposite effect. A particularly striking study in that sense was performed by Smit and Van der Veldt, in which radio-labeled docetaxel was administered before and after bevacizumab to lung cancer patients and traced with a positron emission tomography (PET) scan. In this study, tumor-docetaxel intake significantly decreased after bevacizumab dosing, highlighting the importance of adequate chemo-antiangiogenic scheduling (Van der Veldt et al., 2012). Third, there are many different approved antiangiogenic agents with specificity against different targets (and different Km against each). Each tumor has a unique equilibrium between proangiogenic and antiangiogenic factors that is dynamic over time; hence, the interaction between the drug and one tumor's proangiogenic/antiangiogenic factors may not push the balance in the same direction as in a different one. Thus, it is unlikely that a general statement or model will work for every case. Therefore, personalized case-by-case evaluations should be undertaken.

We hypothesized that tracing the status of vascular normalization could be a realistic option for personalized decisions. We sought to establish the proof-of-principle that ^{18}F-fluoromisonidazole-PET ([18F]-FMISO-PET) can detect in

which tumors vascular normalization is happening, and, in parallel, the amount of chemotherapy being delivered to the tumor is increased. Although not all tumors show the same vascular normality/abnormality status, and although this status may change with time, what seems clear is that when the vasculature is abnormal, the interstitial tissue is hypoxic, secondary to the increased interstitial pressure and edema. If hypoxia could be accurately tracked, then so could vascular abnormality. [18F]-FMISO is a fluorine-labeled, positron-emitting nitroimidazole. After systemic infusion it is reduced and binds to macromolecules within hypoxic cells. It diffuses across cell membranes, showing a passive distribution pattern. At 3 h after infusion, it remains bound only to hypoxic areas, which allows their detection by PET (Bruehlmeier et al., 2004). Baseline and dynamic assessments of tumor hypoxia have shown prognostic correlations in lung and head and neck cancer patients (Eschmann et al., 2005; Gagel et al., 2006; Rischin et al., 2006b). We aimed to test the role of [18F]-FMISO as a potential tracer of vascular normalization. We believe it could be of potential use as a biomarker in the context of antiangiogenic therapy.

Dovitinib is a multi-targeted tyrosine-kinase inhibitor with activity against VEGFR1-3, PDGFRB, and FGFR1-3 that has shown promising preclinical activity in a wide range of tumors. In preclinical models it has demonstrated the capacity for decreasing microvascular density and blocking angiogenesis (Huynh et al., 2012; Lee et al., 2005), because the endothelium is its primary target (Chen et al., 2012). Its vascular-normalizing properties have not been determined, but it is undergoing clinical development for several malignancies. Dovitinib has shown promising activity in preliminary clinical trials, and thus we chose it for our proof-of-concept study.

Taking advantage of a window-of-opportunity (WoO) design, we sought to study whether hypoxia tracing would actually detect the event of vascular re-normalization across different tumors (patient-derived xenografts, PDXs), and whether this phenomenon would be followed by increased interstitial chemotherapy delivery. Controversy exists regarding whether xenografts are excessively prone to develop hypoxia when exposed to antiangiogenics compared to spontaneous cancer models (Franco et al., 2006), and thus not be a perfect model for vascular normalization. Thus, we validated our findings in a genetically engineered mouse model (GEMM) of spontaneous breast cancer.

2. Material and methods

2.1. Mouse models, treatments, and study design

Four-week-old female athymic nude mice were purchased from Charles River Laboratories (Barcelona, Spain). PyMT [FVB/N-Tg(MMTV-PyVT)$^{634Mul/J}$] mice were obtained from W. Muller (McMaster University, Ontario, Canada). All animals were maintained at a constant temperature (24 ± 0.5 °C) under a 12-hour light/dark cycle. All animal experiments were approved by the CNIO Ethics Committee and performed in accordance with the guidelines stated in the International Guiding Principles for Biomedical Research Involving Animals developed by the Council for International Organisations of Medical Sciences.

Patient-derived xenografts (PDX) Panc215 and Panc286 were established and expanded as described previously (Rubio-Viqueira et al., 2006). Tumors from passages 7 and 8 were used for this study.

Gemcitabine hydrochloride (Sigma Aldrich) was freshly prepared in saline and administered at 100 mg/kg per day intraperitoneally twice per week. Dovitinib was freshly prepared in water with a pH of 2.5 and administered at 40 mg/kg per day by oral gavage from days 1–28 and at 20 mg/kg per day subsequently. This dose reduction was undertaken since after 6 weeks of continuous dovitinib administration it was common to observe weight loss (>10%) and vestibular toxicity in approximately 25% of the animals of the combination groups (less frequently, but still observed, in the dovitinib monotherapy animals). By reducing dovitinib to 20 mg/kg after 4 weeks, we did not observe incidence of this toxicity. Gemcitabine was maintained unchanged, since we did not observe signs of cumulative toxicity alone or in combination. Adriamycin was dissolved in PBS and administered at 4 mg/kg intraperitoneally daily for 5 days during the first week.

The study design was a WoO followed by randomized treatment (Figure 1A) (vehicle or dovitinib with or without gemcitabine for the pancreas PDXs, or vehicle, or dovitinib with or without adriamycin for the PyMT animals).

2.2. Tumor measurements and treatment endpoints

Mice were treated until at least one tumor reached approximately 1500 mm^3 (humane endpoint mandating sacrifice). Tumor dimensions were measured twice per week using a caliper, and volumes were calculated using the following formula: $V = (D \times d^2)/2$ mm^3, where D is the largest diameter and d is the shortest diameter. All tumors were measured in one animal and then averaged.

The endpoints under study were tumor growth inhibition (TGI) and overall survival. The first parameter was calculated by using the following formula: $TGI = [1 - (T_F/T_0)_A/(T_F/T_0)_V] \times 100$, where T_F is the tumor volume at the time point analyzed, T_0 is the tumor volume at the initial time, A is the drug or combination undergoing study, and V is vehicle. In order to estimate the overall survival, the dates of treatment start and animal sacrifice (because of reaching the humane endpoint or toxicity) were recorded for each animal; with these values, Kaplan–Meier survival plots were performed (Section 2.6).

2.3. PET-CT imaging studies

Animals were scanned on a small-animal PET scanner (ARGUS PET-CT, SEDECAL, Madrid, Spain) under 3% isoflurane anesthesia. For 2-deoxy-2-^{18}F-fluoro-D-glucose ([18F]-FDG), 0.6 mCi was injected into the tail vein and, after an uptake period of 40 min, animals were scanned for 45 min. For [18F]-FMISO-PET, [18F]-FMISO (0.8 mCi) was injected into the tail vein; after an uptake period of 3.5 h, animals were scanned for 40 min. Both tracers were synthesized by ITP (Instituto Tecnologico PET, Madrid), using an IBA Cyclone C18 cyclotron equipped with an IBA Synthera V2 module with HPLC. Images were reconstructed using a 2D ordered subset expectation maximization algorithm. A tumor region of interest was

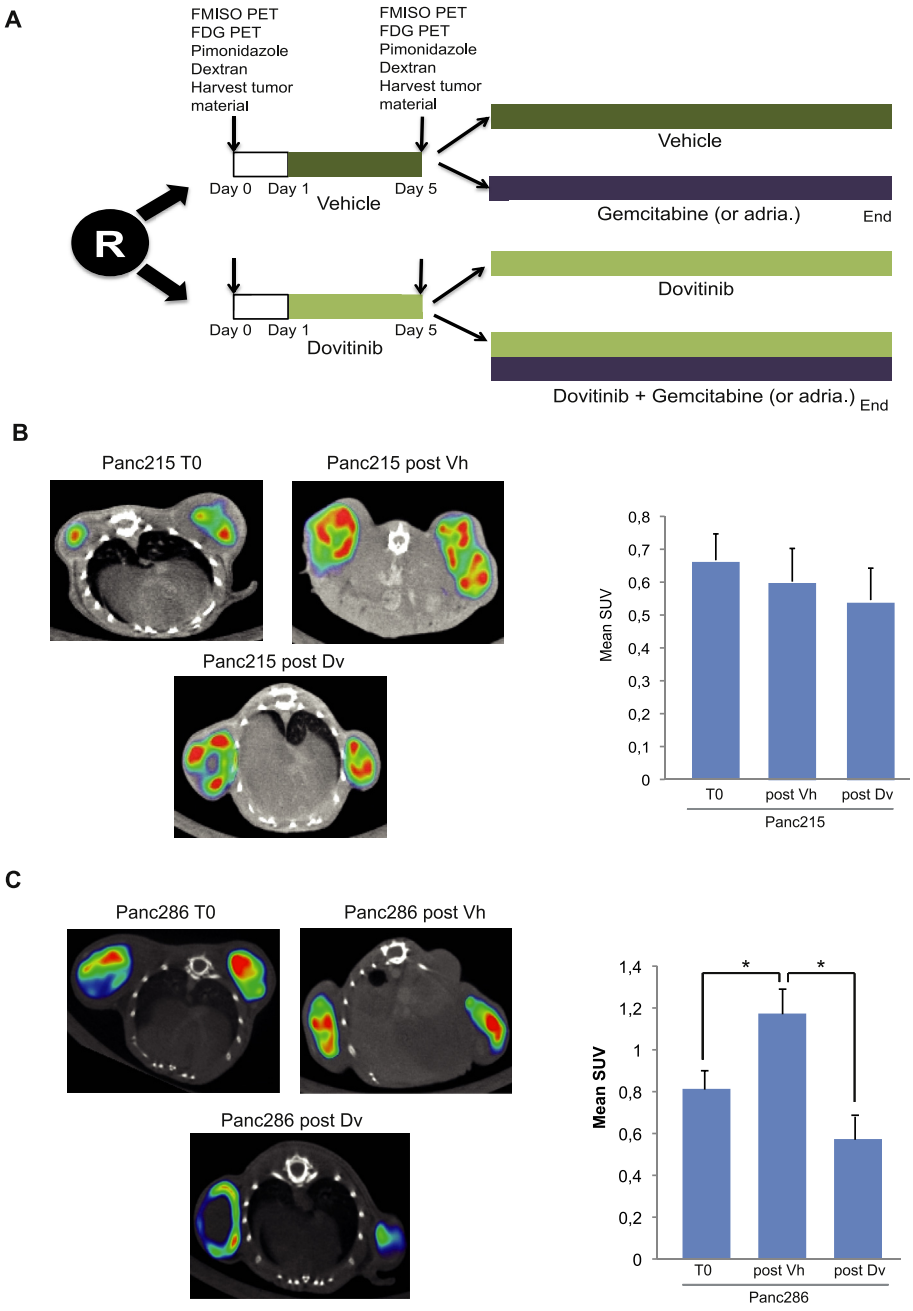

Figure 1 – Treatment schedule and hypoxia evolution during the WoO in pancreas PDXs. (A) Animals were treated during a 5-day window-of-opportunity (WoO) and randomized to either vehicle or dovitinib to assess hypoxia evolution ([18F]-FMISO) and glucose uptake ([18F]-FDG-PET). Treatment groups were set to harvest tumor material for staining microvessels and pimonidazole and for studying dextran extravasation before and after the WoO. Subsequently, the animals were randomized to receiving added gemcitabine or not. Hypoxia evolution by [18F]-FMISO-PET is shown during the WoO of (B) Panc215 and (C) Panc286. Number of tumors assessed per timepoint and condition: Panc215-T0: 11 tumors (6 animals); Panc215-Vehicle-Tend: 9 tumors (5 animals); Panc215-Dovitinib-Tend: 11 tumors (6 animals); Panc286-T0: 12 tumors (6 animals); Panc286-Vehicle-Tend: 9 tumors (5 animals); Panc286-Dovitinib-Tend: 9 tumors (5 animals), Representative scan images are provided. *$P < 0.05$ (*ANOVA-Bonferroni*); error bars: standard error.

manually drawn using coronal, sagittal, and trans-axial sections. The PET data assessment included the analysis of the mean and maximum standard uptake values (SUV_{mean} and SUV_{max}) in the tomographic study. The maximum SUV was the parameter studied for [18F]-FDG. Regarding [18F]-FMISO, the mean SUV was used according to the study by Eschmann *et al* (Eschmann et al., 2007).

2.4. *Histology and immunohistochemistry*

Depending upon the procedure, tumors were fixed in 10% formalin solution, embedded in paraffin, and snap-frozen in isopentane or OCT-embedded for cryopreservation.

Haematoxylin and eosin (H&E) staining was performed according to standard procedures on 3-μm paraffin sections.

Ki67 was stained with a primary anti-Ki67 antibody (clone SP6, Master Diagnostica, Granada, Spain). Cleaved caspase-3 (CC3) was determined with a rabbit antibody from Cell Signaling.

Pimonidazole staining was performed with Hypoxyprobe™-1 Plus kit (HPI Inc, Burlington, MA). Pimonidazole was administered intravenously at 60 mg/kg and tumors were harvested 60 min later. Hypoxyprobe™-1 adducts were detected using an affinity-purified rabbit IgG polyclonal antibody conjugated with horseradish peroxidase following the manufacturer's instructions. Endothelial cells were detected with a rabbit polyclonal antibody against CD31 (Abcam, Cambridge, UK) and were solved with a DBA-conjugated secondary antibody. Tumor tissue hypoxia was quantified as follows: an expert pathologist counted the number of cells positive and negative for pimonidazole staining in three 20X representative fields per slide of three different tumors per timepoint and condition. The evaluated areas included only viable epithelial tissue, and excluded apoptotic areas, stromal-rich areas, or necrotic areas. The scores for each timepoint and condition are presented as percentage of cells positive for pimonidazole.

Slides were scanned at 20X magnification. Digital images were analyzed and quantified with an automated scanning microscope equipped with an image analysis system (Ariol SL-50 with Genetix vs. 3.4.). Necrotic areas were identified and manually drown by an expert pathologist in a minimum of five 4X fields per slide, in three slides per experimental condition; the software calculated the percentage of the analyzed areas that the necrotic areas constituted. Ki67-positive cells, CC3-positive cells, hypoxic and vessel areas were computed to be detected and quantified as percentage of positive cells or percentage of total viable tissue area, by examining a minimum of five 10X fields (Ki67, CC3) or 4X fields (hypoxic areas and vessels).

The dextran-extravasation protocol was performed as follows. Animals were injected intravenously (tail vein) with 10 KDa dextran conjugated with Texas-Red® fluorescent dye 90 min before sacrifice. Tumors were harvested and fixed in 10% formalin solution, embedded in a gradient of sacarose (15% and 30%), embedded in OCT, snap-frozen in isopentane, and stored at −80 °C. Then, 30-μm-thick frozen slides were stained with anti-CD31 antibody (Abcam) and revealed with secondary antibody (Alexa Fluor® 488 goat anti-rabbit IgG, Molecular Probes, Carlsbad, CA). Mounted slides were analysed by confocal microscopy. Six random pictures per tumor were taken at 50× magnification. Quantitation was performed with the Definiens Developer XD software. Dextran extravasation was expressed as the average area of Texas-Red® staining (pixels) divided by the area of blood vessels (CD31-positive pixels) plus the Texas-Red®-positive pixels of five random 40X-fields per tumor from four tumors per timepoint and condition. A value close to 1 indicates important extravasation of the dextran, whereas a value close to 0 indicates that most of the dextran stayed inside the blood vessels or simply has abandoned the tumor as a result of efficient blood flow and lack of blood vessel leakiness. Regarding adriamycin, it was excited with an argon laser at 488 nm; the emission was collected at the 535–600 nm window.

2.5. Intratumoral gemcitabine determination

Calibration standards for gemcitabine were prepared in a 50/50 mixture of acetonitrile and aqueous tetrahydrouridine (THU, Merck Millipore; 200 μg/mL) at concentrations of 25, 50, 75, 100, 250, 500, 750, and 1000 ng/mL. Tumor samples were prepared for gemcitabine analysis by taking 50 μL of the sonicated sample and mixing with 50 μL of MilliQ ultrapure water. The samples were further diluted (1 in 10) for gemcitabine analysis.

Ultraperformance liquid chromatography was performed on a Waters (Milford, MA) iClass Acquity system using a Kinetex C18 (Phenomenex, Torrance, CA) analytical column (150 × 2.1 mm). Mobile phase A included 10 mM ammonium acetate (pH 6.7). Mobile phase B included acetonitrile.

The compounds were eluted isocratically using the 80/20 mix of mobile phases A and B. The column temperature was 30 °C. Mass spectrometry was performed on a Waters TQ-S triple quad mass spectrometer with electrospray ionization. It was operated in positive ion mode for gemcitabine at a source temperature of 150 °C, with desolvation temperature of 650 °C, desolvation gas flow of 800 L/h, capillary voltage of 1.0 kV, source offset of 40 V, cone voltage of 40 V, cone gas flow of 150 L/h, collision energy of 25 V, and collision gas flow of 0.15 mL/min. Data were processed using Waters UNIFI software. Transitions measured were *m/z* 263.9 to 112 for gemcitabine. Linear regression and $1/x^2$ weighting were used for gemcitabine determination.

2.6. Data analysis and statistics

Statistical analysis was performed using SPSS Statistics version 19. Data are shown as mean ± SEM. Percentages were compared with Z-tests. For TGI comparisons, student *t*-test was used for two-group comparisons; three-group comparisons were performed by one-way analysis of variance with Bonferroni test for pairwise comparisons. TGI values were compared at the last timepoint in which the shortest-survival group among those compared still remained animals alive. That timepoint was always the last timepoint plotted in the charts, except for comparisons including vehicle-treated animals in Panc215 (because all the animals were dead at the end of week 2) and comparisons including vehicle-treated animals in the PyMT model (because all animals were dead at the end of week 6). Two-tailed $P < 0.05$ was considered significant.

The effects of the different treatments in animal survival were estimated with the Kaplan–Meier method and the Log-Rank test. When an animal was sacrificed because of reaching the humane endpoint, it was coded as an event. When an animal was sacrificed because of toxicity or tumor-unrelated causes (infection, animal manipulation, dead in cage, etcetera) it was coded as a censured observation. The observation time for each animal lasted from treatment start until sacrifice. Panc286 animals and PyMT animals were followed until all animals required sacrifice because of tumor growth (with the random exceptions of censured events). Panc215 experiment was terminated as two of the treatment groups (gemcitabine and gemcitabine plus dovitinib) showed no visible tumors after 4 weeks of treatment and no visible

changes regarding tumor re-growth were noticed during three additional weeks of observation.

3. Results

3.1. *Baseline hypoxia, hypoxia modulation by dovitinib, and sensitivity to gemcitabine*

We started by tracking hypoxia evolution in the pancreas PDXs. Baseline hypoxia, measured with [18F]-FMISO, was similar in both models (Figure 1B and 1C). Both showed a considerably fast growth pattern (Figure 2A and 2B). However, Panc215 did so without significantly increasing the [18F]-FMISO signal, as opposed to Panc286 (Figure 1B and 1C). The SUV increased by >50% in the vehicle-treated animals in this model. Interestingly, Panc215 was sensitive to gemcitabine, whereas Panc286 was not. Dovitinib alone was not effective in either of the models (Figure 2A and 2B), thus allowing isolation of its potential effect as a vascular normalizing agent without interference with tumor growth. The TGI for dovitinib alone compared to vehicle was 24.0% in Panc215 ($P = 0.14$) and 4.5% in Panc286 (P ANOVA = 1). Dovitinib abrogated hypoxia development in Panc286 during WoO treatment (Figure 1C), but it remained unchanged for the Panc215 group (Figure 1B). In parallel with the abrogation of hypoxia development, dovitinib combined with gemcitabine increased the anti-tumor effects in the Panc286 model (Figure 2B). While gemcitabine alone appeared to enhance tumor growth (it caused a −59.5% TGI, or, in other words, 59% increase in tumor size), and dovitinib alone had no effect, the combination

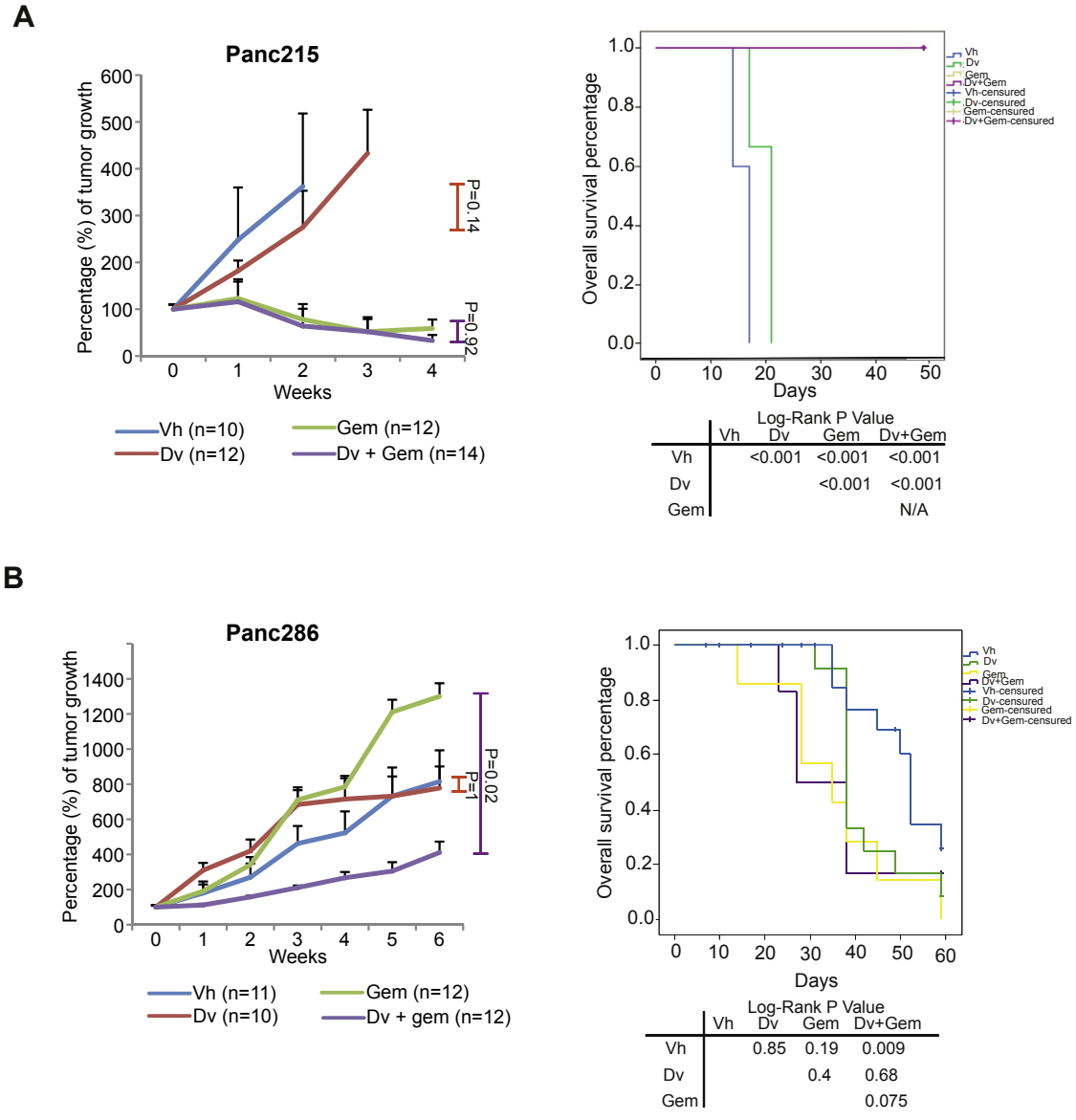

Figure 2 – Tumor growth of Panc215 and Panc286. The left charts indicate the growth of the (A) Panc215 and (B) Panc286 PDXs treated with vehicle, dovitinib, or gemcitabine, or both dovitinib and gemcitabine. The Kaplan–Meier survival curves for the same treatment groups are shown in the right panels. Error bars: standard error.

provided significant inhibition relative to the vehicle controls [49.6% TGI; *P*-value (T-test) for gemcitabine+dovitinib versus gemcitabine = 0.02]. Conversely, although Panc215 was already sensitive, the addition of dovitinib did not add any further benefit to gemcitabine (Figure 2A) [TGIs: gemcitabine, 78.4%; gemcitabine plus dovitinib, 82.3%; *P*-value (T-test) for gemcitabine+dovitinib versus gemcitabine = 0.92]. The Kaplan–Meier estimates for median overall survival of the different treatment groups yielded similar effects. Regarding Panc215, the median overall survival times for vehicle- and dovitinib-treated groups were 17 and 21 days respectively, whereas it was not reached for the other two groups (Log-Rank $P < 0.001$). At 28 days, the tumors had virtually disappeared for the gemcitabine- and dovitinib plus gemcitabine-treated animals; we observed the animals for 3 more weeks and since no tumor re-growth was observed, the experiment was terminated (Figure 2A). Finally, regarding Panc286, the median overall survival times were 35 (vehicle), 27 (dovitinib), 38 (gemcitabine) and 52 (dovitinib plus gemcitabine) days (Log-Rank $P < 0.001$, Figure 2B).

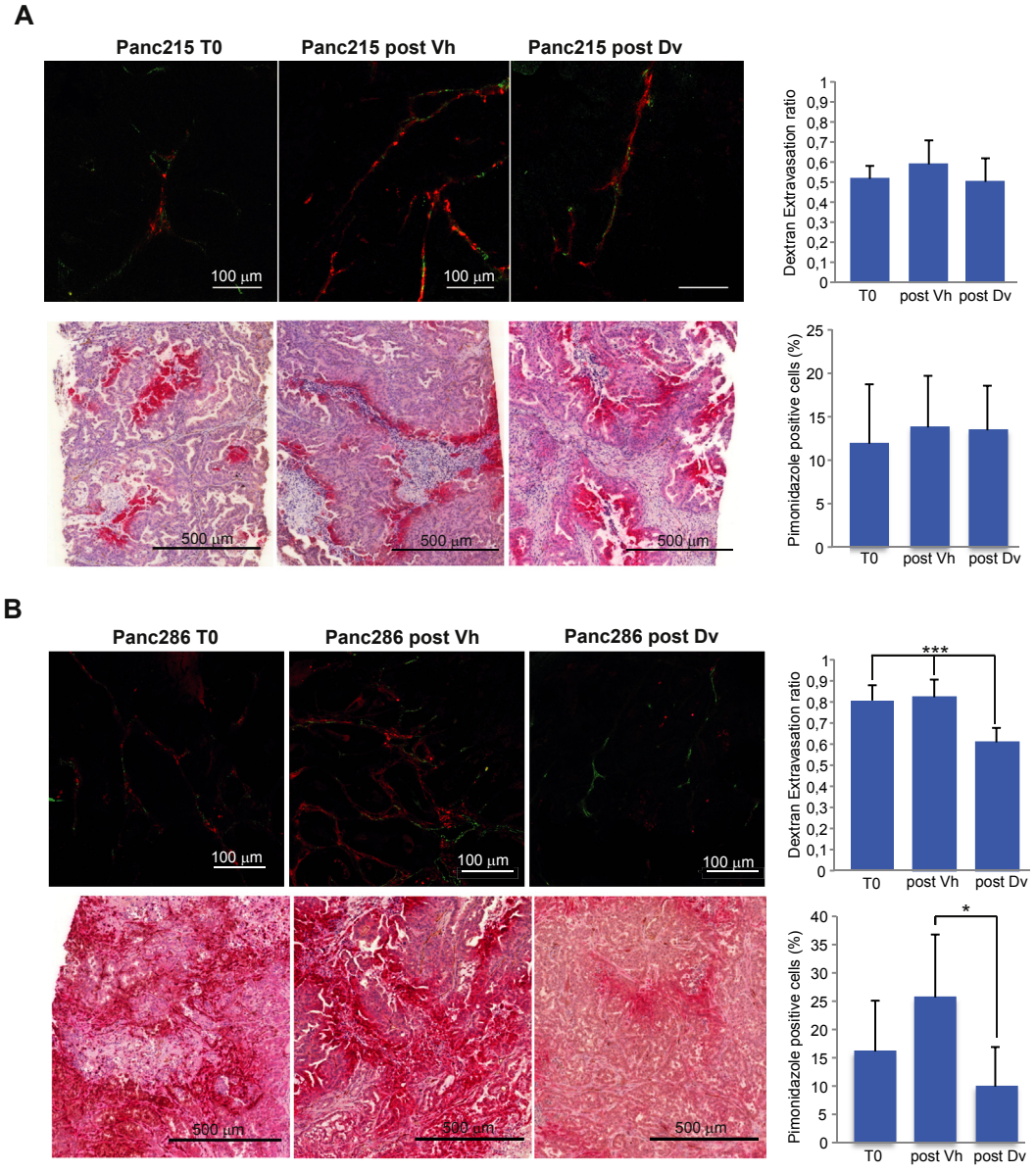

Figure 3 – [18F]-FMISO tracks vascular normalization. In the upper panels, confocal staining of microvessels with CD31 (green) and perivascular 10 KDa dextran (red) is shown, either before treatment (left) or after the WoO with vehicle (middle) or dovitinib (right). In parallel, we show the immunohistochemistry of pimonidazole (red) at the same timepoints (lower panels). It can be appreciated how in Panc215 (A) there is virtually no change during the WoO regardless of whether vehicle or dovitinib is administered. The hypoxic areas are not modified either. The charts represent, respectively, the ratio between the area positive for dextran (inside and outside blood vessels) and the area positive for dextran plus the blood vessels area (upper chart), and the percentage of cells positive for pimonidazole (lower chart, *P*-ANOVA = 0.88). (B) On the contrary, dovitinib treatment induces a change in the microvasculature so that there is no longer extravasation of dextran (right inset). The chart numerically represents this descent (*P*-ANOVA = 0.004). In parallel, there is a correction of hypoxia, as evidenced by the decreased red-staining in the images and the values plotted in the chart. *Z-test $P = 0.016$. Error bars: standard error of the mean.

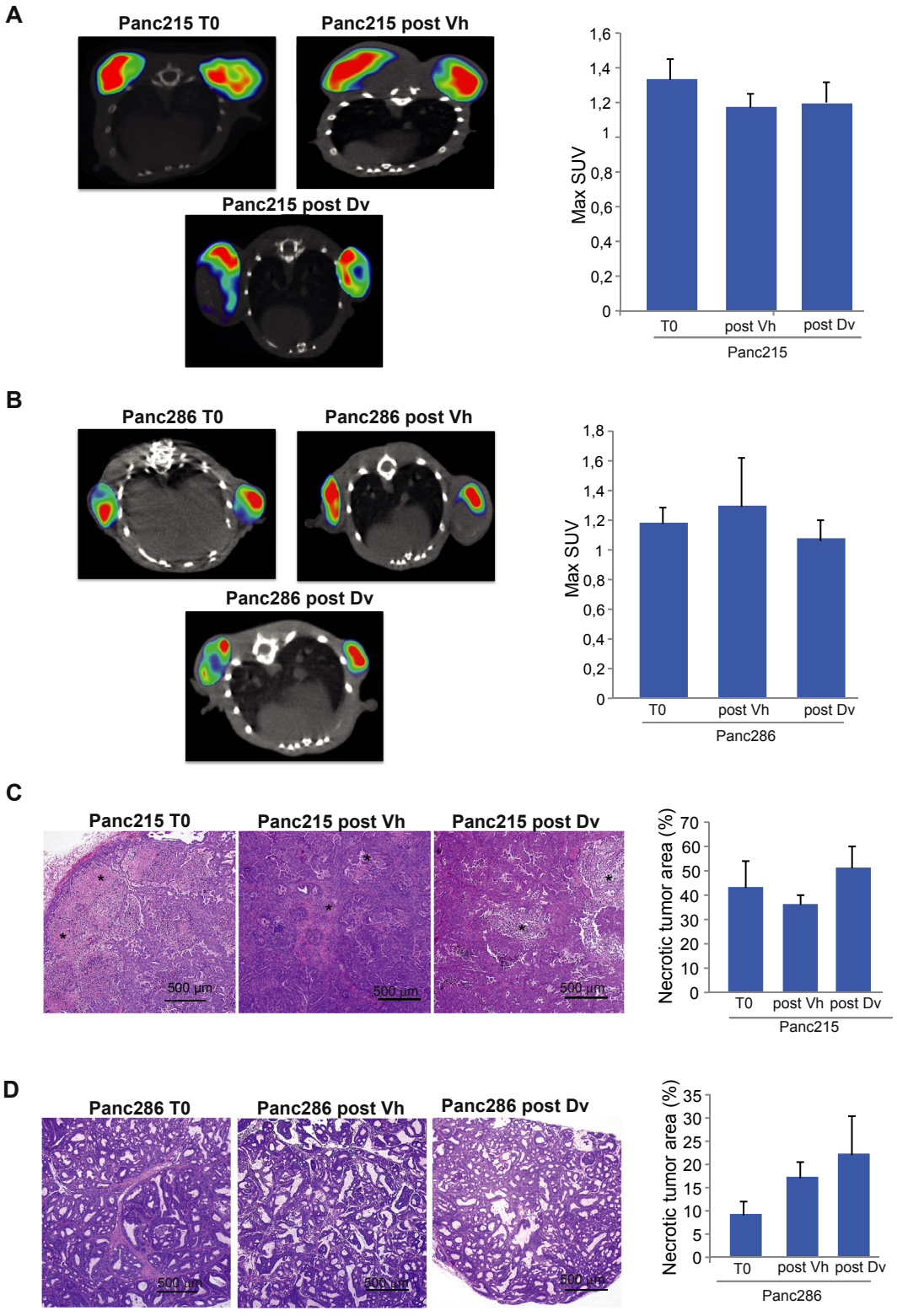

Figure 4 – Decreased [18F]-FMISO uptake does not correspond to necrotic areas. [18F]-FDG-PET before and after the WoO with vehicle or dovitinib plus quantitation of the maximum SUV (n = 10 tumors) for (A) Panc215 or (B) Panc286. *P* = 0.31 and 0.53, respectively (Bonferroni). Thus, despite the lack of changes in viability or glucose avidity, [18F]-FMISO showed dovitinib-induced changes. Representative H&E images during the WoO for (C) Panc215 and (D) Panc286, respectively, where necrosis has been marked with asterisks. The necrosis percentage was quantified as total area in three independent tumor sections; this percentage was very low for Panc286. In both cases, it did not suffer significant variations during the WoO (*P* = 0.29 and 0.14, respectively; *Bonferroni*).

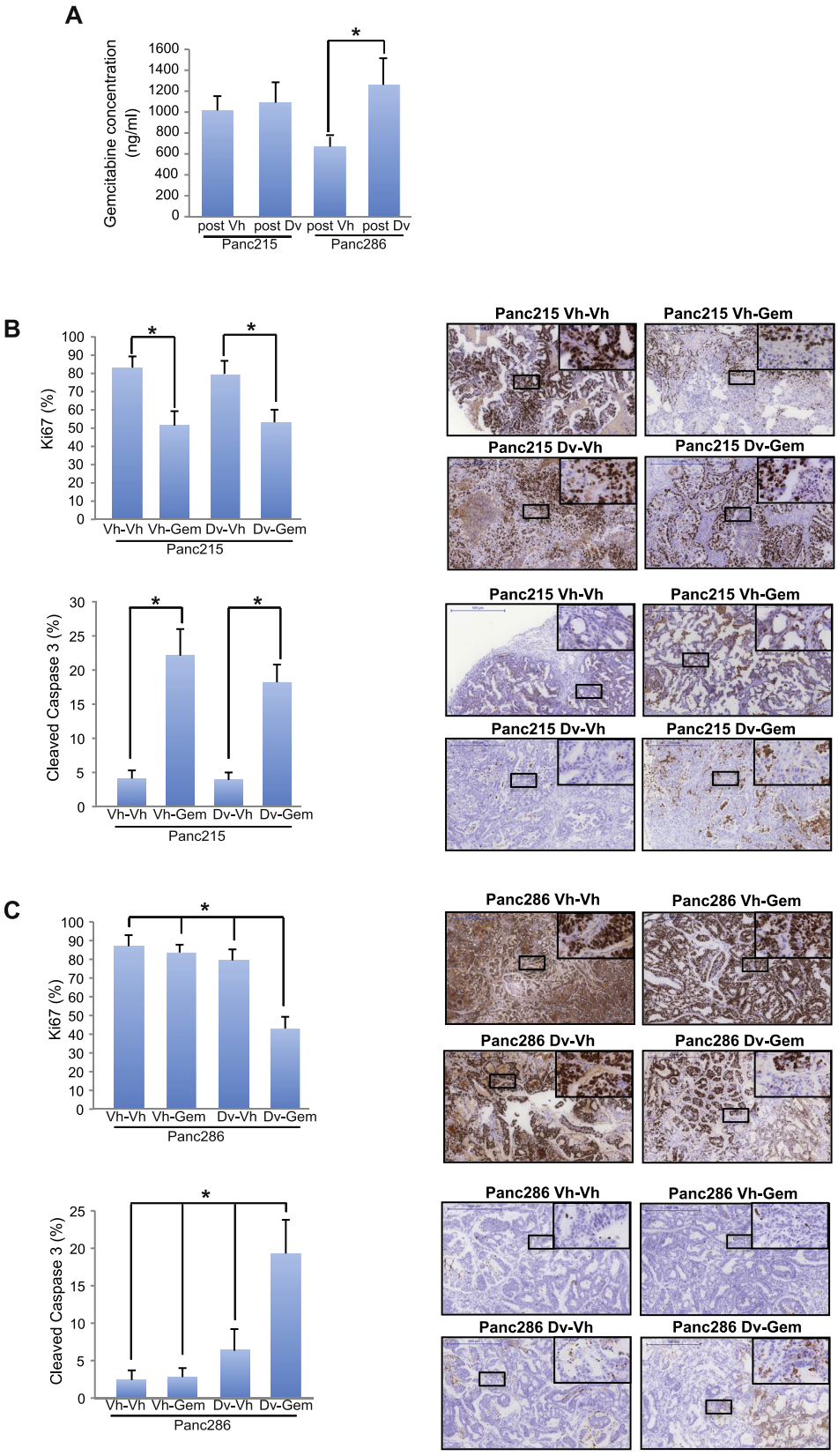

Figure 5 – [18F]-FMISO tracks increased chemotherapy delivery and sensitivity secondary to vascular normalization. (A) Chart depicts the intratumor concentration of gemcitabine recovered 5 min after injection from 215 to 286 PDXs, either after a WoO with vehicle ("post-Vh") or dovitinib ("post-Dv"). The numbers of tumors were 10, 8, 8, and 10 for 215 post-Vh, 215 post-Dv, 286 post-Vh, and 286 post-Dv, respectively (two tumors were grafted per animal, but usually 1 or 2 tumors per group fail grafting). (B) Ki67 (left, upper) and CC3 (left, lower) percentages in Panc215 after a single dose of vehicle following vehicle during the WoO ("Vh-Vh") or a single dose of gemcitabine following vehicle during the

3.2. [18F]-FMISO evolution tracks vascular normalization

The concept of vascular normalization establishes that the increased effects of chemotherapy when combined with an antiangiogenic agent are mediated by improved vessel functionality. The extravasation of high-molecular-weight dextrans is a good parameter for monitoring vascular abnormality (high extravasation means vascular abnormality). We monitored extravasation of 10 KDa Texas-Red dextran in the proximity of blood vessels during WoO to determine if [18F]-FMISO-PET was monitoring its evolution.

Perivascular dextran extravasation remained stable during vehicle-WoO treatment in Panc215 (Figure 3A, upper panels and chart) and Panc286 (Figure 3B, upper panels and chart). Dovitinib, which was able to reduce [18F]-FMISO SUV in Panc286, was able to reduce perivascular extravasation in Panc286 during WoO, but not in Panc215 (Figure 3A and 3B, upper panels and charts). Thus, [18F]-FMISO evolution mirrors the extravasation of 10 KDa dextran in these two models.

We aimed to determine if hypoxia and dextran extravasation also followed parallel behavior at the microscopic level. We co-stained pimonidazole (a probe that binds to areas with $<1\%$ O_2) and microvessels. The images shown in the lower panels in Figure 3A and 3B suggest hypoxia reversion (Figure 3B, lower) accompanies vessel normalization (Figure 3B, upper); when vessels are not normalized (Figure 3A, upper), hypoxia is not corrected (Figure 3A, lower; Panc215). The percentage of cells positive for pimonidazole remained stable ($\sim$15%) in Panc215 tumors from before to after the WoO, both in the vehicle- and dovitinib-treated animals. However, in Panc286 tumors, we observed a statistically significant decrease in the hypoxic cells fraction (25.6%–9.8%; $P = 0.016$) in the dovitinib-treated animals. Both pimonidazole and [18F]-FMISO are 2-nitroimidazole hypoxia probes that bind to hypoxic tissue through the same mechanism; thus it was expected that we obtained similar results with both techniques. However, it was necessarily to validate that we could obtain with a non-invasive technique the same readout as with pimonidazole, and thus, we had to demonstrate that the external PET-imaging was adequately capturing hypoxia changes at the microscopic level. According to these results, [18F]-FMISO-PET is tracking hypoxia, a surrogate parameter of vascular normalization.

Finally, numerical assessment of microvessels does not necessarily translate to vessel functionality or adequate perfusion (i.e., vascular normalization), as pointed out by Judah Folkman in 2002 (Hlatky et al., 2002). Although in that work the risks of the assessment of microvessel density as a potential parameter that could work as a biomarker of efficacy of antiangiogenics were thoroughly discussed, this parameter is commonly reported in studies and trials of antiangiogenics. Dovitinib induced a slight, but statistically significant, decrease in microvessel density during WoO treatment in Panc286 (Figure S1). Conversely, the changes induced by either vehicle or dovitinib in Panc215 did not reach statistical significance (Figure S1).

Taken together, these data suggest that [18F]-FMISO-PET tracks the process of antiangiogenic-induced vascular normalization during WoO treatment.

3.3. Specificity of [18F]-FMISO and tissue viability

Dovitinib could be inducing tumor necrosis secondarily to potential vascular-pruning effects, which could affect the potential assessment of TGI. In addition, necrosis is not adequately assessed by [18F]-FMISO (because [18F]-FMISO binding is dependent on metabolic viability of the cells, and thus it does not bind to necrotic areas (Bruehlmeier et al., 2004) – hence, it would be difficult to know whether a decrease in [18F]-FMISO uptake was caused by increased necrosis, or by an increased normoxic tumor fraction that is not avid for [18F]-FMISO). We aimed to confirm whether the signal changes shown in Figure 1 corresponded to oxygenation changes (and, thus, vascular normalization), or whether the tissue simply became necrotic and the tracer was not proficient in detecting this parameter.

We performed [18F]-FDG-PET during the WoO in both PDXs (Figure 4A and 4B); as opposed to [18F]-FMISO, necrotic areas can be detected by [18F]-FDG as "black" areas. It can be clearly appreciated that the tissue is viable and glucose-avid in both cases, with no meaningful changes over time with vehicle or dovitinib treatment. We also determined the necrotic areas with H&E staining and histologic evaluation. Again (Figure 4C and 4D), we confirmed the lack of induction of necrosis by antiangiogenic treatment during the WoO. We can thus conclude that the changes in the [18F]-FMISO signals were specific to viable tissue.

3.4. Normalized tumors tracked by [18F]-FMISO show increased gemcitabine concentration and cell death in response to gemcitabine

Cytotoxicity and/or chemo-sensitivity are multifactorial features of epithelial malignancies. However, two important factors that influence chemo-sensitivity are the amount of drug that is delivered and microenvironmental hypoxia. [18F]-FMISO-PET seems to trace hypoxia (Figures 1 and 3). We also measured interstitial gemcitabine in both tumor models. Animals harboring the Panc215 PDX were treated during the WoO with either vehicle or dovitinib and then given a single dose of gemcitabine. The average intratumor concentration of gemcitabine (harvested 5 min after the injection) was virtually the same in both groups (1015 and 1089 ng/mL, respectively; Figure 5A), showing that the lack of changes in [18F]-FMISO signal and vascular normalization accompanied a lack of changes in drug delivery. However, in the case of Panc286, the results were different. After vehicle-WoO treatment, the tumors had an average gemcitabine concentration of 665 ng/mL, which almost doubled after dovitinib-WoO

WoO ("Vh-Gem"), or after a single dose of vehicle or gemcitabine following dovitinib during the WoO ("Dv-Vh" and "Dv-Gem," respectively). Representative insets of Ki67 (right, upper) and CC3 (right, lower) staining (upper left: Vh-Vh; upper right: Vh-Gem; lower left: Dv-Vh; lower right: Dv-Gem). (C) Same charts and insets for Panc286. *$P < 0.05$ (*ANOVA-Bonferroni*); error bars: standard error.

treatment (Figure 5A). These data suggest that [18F]-FMISO tracks vascular normalization and increased drug delivery in the interstitium, which could explain the increased efficacy of gemcitabine combined with dovitinib compared to gemcitabine alone in Panc286.

The Ki67 fraction decreased and the CC3 staining increased after a single post-vehicle WoO-gemcitabine dose (compared to baseline parameters) in the Panc215 PDX, but these parameters were not modified by the dovitinib-WoO (Ki67 and CC3 assessed 48 h after the gemcitabine dose). The single gemcitabine dose induced similar changes in Ki67 and CC3 (Figure 5B). As expected, gemcitabine only modified these parameters after dovitinib priming (Figure 5C) in Panc286.

3.5. *Validation in the PyMT genetically engineered mouse model of breast cancer*

It has been proposed that xenografts might be excessively prone to develop hypoxia due to three factors: the fact that xenografts grow subcutaneously and are poorly vascularized, the lack of immune system (which is a main regulator of the angiogenesis process), and the species mismatch between stroma and parenchyma (Sharpless and Depinho, 2006). Therefore, the vascular normalization phenomenon might not work exactly the same as in spontaneous tumors (Francia et al., 2011; Kerbel, 2011, 2012; Kerbel et al., 2013). We sought to validate our findings in an independent model. We backcrossed the MMTV-PyMT breast cancer model to a pure FVB background which gave rise to ductal carcinoma *in situ* of the breast at 4 weeks of age; at 7 weeks of age, 100% of animals had invasive tumors that were, on average, approximately 150 mm^3 (Figure S2). When starting treatment at this age, the tumors were resistant to adriamycin, the most widely used chemotherapy agent against breast cancer (TGI adriamycin vs. vehicle: 2.8%; T-test $P = 0.74$) (Figure 6A). Dovitinib alone was able to induce significant effects in TGI (49.8% TGI; $P < 0.001$). The combination of dovitinib plus adriamycin was the most powerful; however, it only achieved statistical significance for the comparison versus adriamycin monotherapy and not versus dovitinib alone (TGI of adriamycin plus dovitinib: 63.5%; T-test *P* value for adriamycin versus adriamycin+dovitinib <0.001; *P* value for dovitinib versus adriamycin+dovitinib = 0.16) (Figure 6A). In terms of animal survival, the different treatment groups yielded the following results: vehicle, 28 days; adriamycin, 35 days; dovitinib, 49 days; dovitinib plus adriamycin, 63 days (Log-Rank $P < 0.001$) (Figure 6A). After the dovitinib-WoO, compared with vehicle, [18F]-FMISO uptake was reduced by approximately 50% (Figure 6B). [18F]-FMISO uptake mirrored hypoxia evolution at the microscopic level (Figure 6C), showing how dovitinib corrected this parameter. The percentage of cells positive for pimonidazole was 30.6% in the vehicle-treated animals, compared to 3.6% in the dovitinib-treated animals (Z-test $P < 0.001$) (Figure 6C). The confocal images in Figure 6D show how the delivery of adriamycin (which has the advantage over gemcitabine of emitting red fluorescence) is increased in the vascular/perivascular areas after the dovitinib-WoO compared with vehicle. As opposed to large molecules (i.e., 10 Kda dextrans), that, when present in the perivascular areas indicate abnormal vessel function and poor perfusion, the increased presence of small molecules in the vascular/perivascular such as fluorescent lectins (or adriamycin) is indicative of improved perfusion (Rolny et al., 2011). Finally, at a higher magnification, it can also be appreciated how adriamycin is bound to the nuclei of cancer cells in the dovitinib-treated animals (Figure S3, lower panels), as opposed to the vehicle-treated tumors (S3, upper panels), where the arrival of adriamycin to the nuclei is very poor.

4. Discussion

Although there is previous work analyzing the perfusion changes in response to antiangiogenic treatment (Ferl and Port, 2012; Jain, 2013a), finding predictive factors or biomarkers for the activity of antiangiogenic agents has been an elusive task. Chemotherapy sensitivity is modulated by co-administration of antiangiogenic drugs (Jain, 2005, 2013b; Kerbel, 2006). According to the theory of vascular normalization, tumors have abnormal vessels that impede adequate delivery of chemotherapy drugs (Jain, 2005, 2013b; Kerbel, 2006). Antiangiogenics alone would not cause meaningful antitumor effects, but rather would facilitate the delivery of chemotherapy and re-oxygenate the interstitium, which would also increase the chemo-sensitivity (Jain, 2005, 2013b; Kerbel, 2006). Obviously, this would not occur in a uniform manner, as evidenced by the fact that not all the patients enrolled in chemotherapy plus antiangiogenic trials experience a clinical response (Jain, 2008). In addition, contradictory reports exist on whether antiangiogenics improve or deteriorate perfusion (Van der Veldt et al., 2012). We proposed that because abnormal blood vessels are accompanied by hypoxic interstitium, tracking hypoxia would allow tracking vascular normalization with an available noninvasive biomarker.

We show how the same antiangiogenic agent, dovitinib, does not necessarily induce a homogeneous normalizing effect across tumors of the same type. In our study, dovitinib was able to normalize Panc286 (Figure 3B), but not Panc215 (Figure 3A). The balance between proangiogenic and antiangiogenic factors is specific to a given tumor in a given moment and is dynamic in nature. It is not realistic to expect that two tumors from two different patients will have the same balance and that they will be constant over time. In addition, the effects of a drug with pleiotropic effects (such as dovitinib, with therapeutic effects in at least eight kinases) are the result of the interaction of the drug with the specific balance of a specific tumor and are probably difficult to predict. However, as shown in Figures 1B, 1C, and 4, they seem traceable. What is of key importance about tracing dovitinib effects is not hypoxia itself (although hypoxia is a tumor progression factor), but rather the fact that hypoxia seems to be a surrogate parameter of vascular abnormality. When hypoxia is reverted (Figures 1C and 3B), so is abnormality (Figure 3B). What is more important for the clinical applicability is that when this phenomenon occurs, chemotherapy delivery is improved (Figure 5A) and cytotoxicity is enhanced (Figure 5C). Conversely, when hypoxia is not corrected (Figures 1B and 3A), the abnormality is not reverted (Figure 3A). In this situation, dovitinib does not modify the amount of interstitial gemcitabine or cytotoxicity (Figure 5A and 5B). All these microscopic effects had accurate

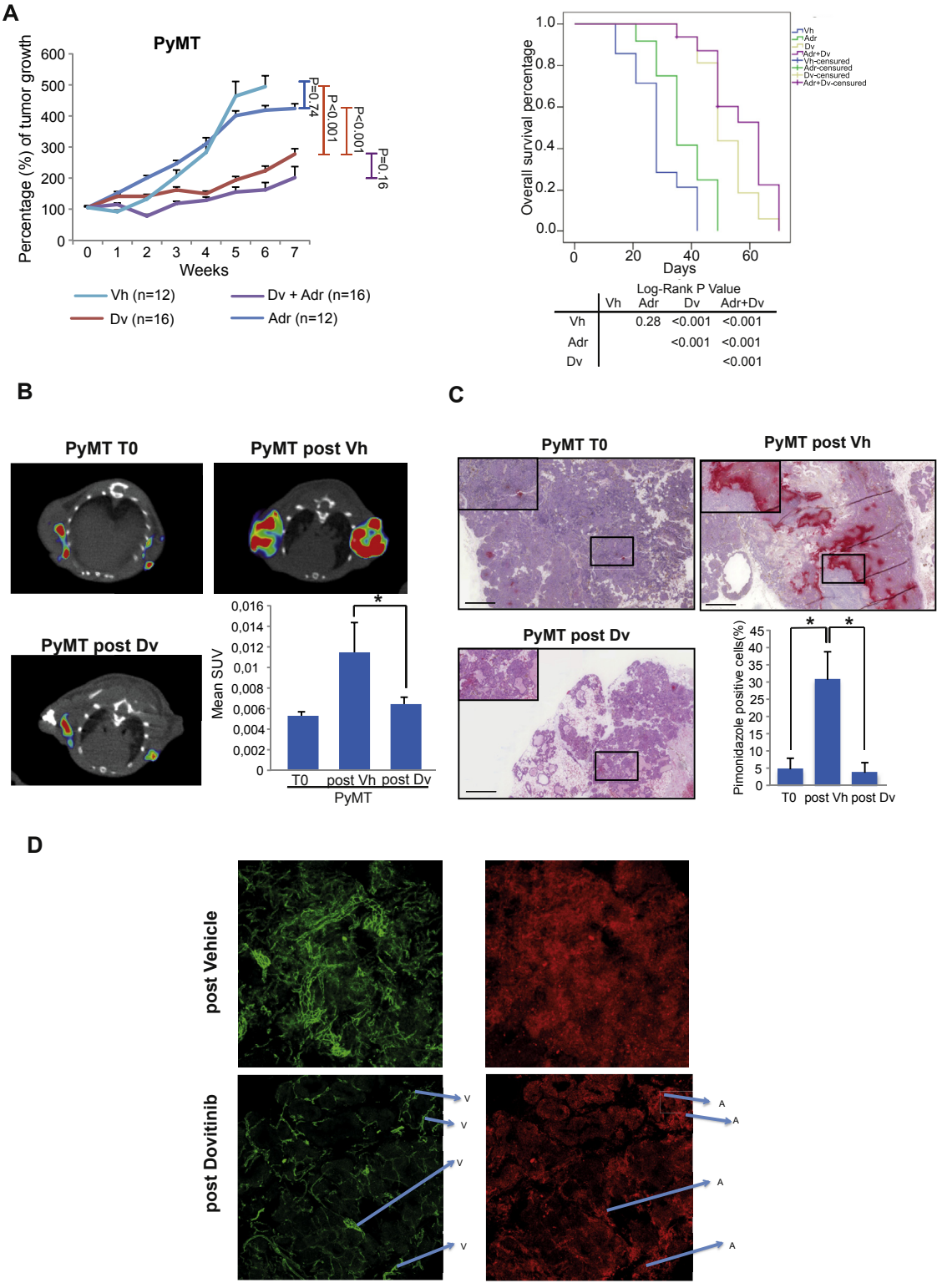

Figure 6 – Validation in the PyMT genetically engineered breast cancer model. (A) Tumor growth and survival of the PyMT tumors/animals in response to the four treatments. (B) [18F]-FMISO suggests decreased hypoxia after a WoO with dovitinib compared to vehicle (T-test $P < 0.001$). (C) Pimonidazole staining showing hypoxia evolution in response to dovitinib or vehicle plus quantitation chart (*Z-test $P < 0.001$). (D) CD31 staining (left panels) is shown from representative tumors after the WoO with vehicle (up) or dovitinib (down). The number of vessels decreases, and the vessel trajectory is less tortuous; also the vessel size is homogeneous and regular along the vessel course. On the right side, the fluorescence captured by the red-light filter is shown. Interestingly, the bright signal characteristic of adriamycin is highlighted over the background delineating the trajectory of blood vessels, indicating perfusion of the tumors and arrival of the agent. Conversely, no pattern can be recognised in the upper panel. In order to facilitate the identification, the vessels are labelled as "V" and the corresponding areas with bright adriamycin signal as "A" in the bottom panels. Error bars: standard error of the mean.

translation in TGI (Figure 2). Taken together, the results suggest that [18F]-FMISO mirrors the combined evolution of hypoxia and vascular normality/abnormality in response to short-course antiangiogenic treatment. The results seem to be valid both in the pancreas cancer PDXs and the breast cancer GEMM. It is important to mention, however, that we have not established a causal link between [18F]-FMISO signal changes and chemo-sensitization. Sensitivity to chemotherapy is a complex phenomenon; many factors play a role in chemosensitivity. Of those, chemotherapy concentration is only one of them. We only provide proof-of-principle results regarding how [18F]-FMISO monitors the changes in the interstitium that accompany vascular normalization, which, in our models, was followed by increased chemotherapy delivery. Increased chemotherapy delivery or concentration may or may not be followed by increased tumor cell death, despite the fact that we offer examples of a positive correlation (Figure 5C). A causal link between [18F]-FMISO signal changes and subsequent chemo-sensitization will only be possible to establish when many tumor models, or, preferably, patients, are analyzed.

The WoO is not aimed to or sufficient to re-sensitize the tumors to chemotherapy. Both the breast and the pancreas models that were insensitive to adriamycin or gemcitabine monotherapy but were sensitive to the combinations required continuous treatment of chemotherapy plus dovitinib until sacrifice. In fact, we tested treatment groups consisting on dovitinib 5 days followed by vehicle plus chemotherapy, and the results were virtually identical to vehicle plus chemotherapy groups (data not shown). The WoO is aimed to show that the antiangiogenic is able to induce stromal changes (decrease dextran extravasation, improved chemotherapy delivery, decrease hypoxia and improved vessel architecture), and allows demonstrating that [18F]-FMISO-PET is able to monitor these changes. The early detection of these changes by [18F]-FMISO-PET may allow having available a tool with predictive power in the clinical setting, regardless of whether is the baseline hypoxia or the hypoxia levels after a few days or at the end of the treatment course what predicts the sensitivity – such information will only be answered within a clinical trial. However, what seems reasonable is to state that chemotherapy sensitivity requires vascular normalization and chemotherapy delivery, and that [18F]-FMISO-PET is able to indirectly detect that by measuring interstitial hypoxia.

Two important advantages of this type of testing are its noninvasiveness and its quantitative nature in "real time." Baseline and dynamic assessment of tumor hypoxia have shown prognostic correlation in lung and head and neck cancer patients (Eschmann et al., 2005; Rischin et al., 2006a). We tested its role as a tool for tracing the positive effects of antiangiogenics. The results seem to be specific and not biased, at least in this study, by necrotic tumor areas. The expression of reductases can affect the binding of hypoxic probes in tissues (Wang et al., 2012), but we did not find changes in CYPOR reductase expression in tumors treated with dovitinib or vehicle that could justify the different [18F]-FMISO uptake after the WoO in the different models (data not shown). An obvious limitation of our study is that it needs to extend the observations to further models and/or drugs, but we simply aimed to provide proof of principle. According to our hypothesis, the effects of a given antiangiogenic drug might be normalizing in one tumor and "abnormalizing" in another; similarly, two antiangiogenic drugs might exert different normalizing/abnormalizing effects in the same tumor because of their different affinities against various receptors. However, the ultimate effects in the interstitium (normalization and, in parallel, oxygenation) and its downstream consequences (increased chemotherapy delivery) seem to be easily monitorable according to our study and should not depend upon the agent used. A clinical trial with many patients will provide stronger evidence to our proof-of-principle than further mouse models. We have recently completed a randomized clinical trial based upon this concept, and it is currently undergoing analysis. The patients were treated with a similar agent (nintedanib); and a positive result in this trial would confirm the hypothesis that vascular normalization can be traced in an individual basis with [18F]-FMISO-PET.

5. Conclusions

Although there is previous work evaluating the role of other imaging techniques (mainly DCE-MRI) in predicting the outcome of patients treated with antiangiogenics (Ferl and Port, 2012; Jain, 2013a), unfortunately it is still complex to incorporate such techniques in the daily-routine clinical decision-trees. Since antiangiogenics may exert their positive effect by normalizing the stroma, at least in some cases, and abnormal stroma is characterized by hypoxia, we sought to monitor hypoxia evolution in several tumor models exposed to the antiangiogenic agent dovitinib. We demonstrate how [18F]-FMISO-PET is able to detect when dovitinib is exerting a positive effect in the stroma. When [18F]-FMISO-PET signal decreases, so does tissue hypoxia. In parallel, the vascular structures are normalized and the delivery of chemotherapy (administered in combination with dovitinib) to the interstitium increases, what is followed by increased tumor cell death Thus, [18F]-FMISO-PET is a potential tool that could detect in an individual basis when antiangiogenic tumors are inducing vascular normalization.

Disclosure of potential conflicts of interest

MQF has been the principal investigator of a phase I trial conducted with dovitinib and received research funds from Novartis.

Author contribution

- Conception, design and study supervision: Miguel Quintela-Fandino and Manuel Desco.
- Development of methodology: Elena Hernandez-Agudo, Marisa Soto-Montenegro, Diego Megias, Jesus Sanchez, Tamara Mondejar, Silvana Mouron, Pedro Pablo Lopez-Casas, Francisca Mulero.
- Acquisition of data: Elena Hernandez-Agudo, Marisa Soto-Montenegro, Diego Megias, Jesus Sanchez, Tamara Mondejar, Silvana Mouron, Francisca Mulero.

- Analysis and interpretation: Elena Hernandez-Agugo, Marisa Soto-Montenegro, Diego Megias, Manuel Hidalgo, Manuel Desco, Miguel Quintela-Fandino.
- Writing of the manuscript: Elena Hernandez-Agudo, Marisa Soto-Montenegro, Manuel Desco, Miguel Quintela-Fandino.

Acknowledgments

This work was supported by the following sources: Fondo de Investigación Sanitaria (Ministry of Health, Spain; numbers FIS PI10/0288, FIS PI13/00430, FIS PI 11/00616, CPII14/00005 and FIS PI14/00860; the first two awarded to MQF and the last three to MD), and "Fondo Europeo de Desarrollo Regional (FEDER) – Una manera de hacer Europa". MQF is a recipient of a 2010 Beca-Retorno from the AECC Scientific Foundation. Rosae Foundation and AVON España S.A.U. contributed to this work with unrestricted donations. Dovitinib was kindly provided by Novartis.

Appendix A. Supplementary data

Supplementary data related to this article can be found at http://dx.doi.org/10.1016/j.molonc.2015.12.011.

REFERENCES

Bruehlmeier, M., Roelcke, U., Schubiger, P.A., Ametamey, S.M., 2004. Assessment of hypoxia and perfusion in human brain tumors using PET with 18F-fluoromisonidazole and 15O-H2O. J. Nucl. Med. 45, 1851–1859.

Burger, R.A., Brady, M.F., Bookman, M.A., Fleming, G.F., Monk, B.J., Huang, H., Mannel, R.S., Homesley, H.D., Fowler, J., Greer, B.E., Boente, M., Birrer, M.J., Liang, S.X.Gynecologic Oncology, G, 2011. Incorporation of bevacizumab in the primary treatment of ovarian cancer. N. Engl. J. Med. 365, 2473–2483.

Chen, Z.Y., Shi, M., Peng, L.X., Wei, W., Li, X.J., Guo, Z.X., Li, S.H., Zhong, C., Qian, C.N., Guo, R.P., 2012. Dovitinib preferentially targets endothelial cells rather than cancer cells for the inhibition of hepatocellular carcinoma growth and metastasis. J. Transl Med. 10, 245.

Cobleigh, M.A., Langmuir, V.K., Sledge, G.W., Miller, K.D., Haney, L., Novotny, W.F., Reimann, J.D., Vassel, A., 2003. A phase I/II dose-escalation trial of bevacizumab in previously treated metastatic breast cancer. Semin. Oncol. 30, 117–124.

Eschmann, S.M., Paulsen, F., Bedeshem, C., Machulla, H.J., Hehr, T., Bamberg, M., Bares, R., 2007. Hypoxia-imaging with (18)F-Misonidazole and PET: changes of kinetics during radiotherapy of head-and-neck cancer. Radiother. Oncol. 83, 406–410.

Eschmann, S.M., Paulsen, F., Reimold, M., Dittmann, H., Welz, S., Reischl, G., Machulla, H.J., Bares, R., 2005. Prognostic impact of hypoxia imaging with 18F-misonidazole PET in non-small cell lung cancer and head and neck cancer before radiotherapy. J. Nucl. Med. 46, 253–260.

Ferl, G.Z., Port, R.E., 2012. Quantification of antiangiogenic and antivascular drug activity by kinetic analysis of DCE-MRI data. Clin. Pharmacol. Ther. 92, 118–124.

Folkman, J., 1971. Tumor angiogenesis: therapeutic implications. N. Engl. J. Med. 285, 1182–1186.

Francia, G., Cruz-Munoz, W., Man, S., Xu, P., Kerbel, R.S., 2011. Mouse models of advanced spontaneous metastasis for experimental therapeutics. Nat. Rev. Cancer 11, 135–141.

Franco, M., Man, S., Chen, L., Emmenegger, U., Shaked, Y., Cheung, A.M., Brown, A.S., Hicklin, D.J., Foster, F.S., Kerbel, R.S., 2006. Targeted anti-vascular endothelial growth factor receptor-2 therapy leads to short-term and long-term impairment of vascular function and increase in tumor hypoxia. Cancer Res. 66, 3639–3648.

Gagel, B., Reinartz, P., Demirel, C., Kaiser, H.J., Zimny, M., Piroth, M., Pinkawa, M., Stanzel, S., Asadpour, B., Hamacher, K., Coenen, H.H., Buell, U., Eble, M.J., 2006. [18F] fluoromisonidazole and [18F] fluorodeoxyglucose positron emission tomography in response evaluation after chemo-/radiotherapy of non-small-cell lung cancer: a feasibility study. BMC Cancer 6, 51.

Gilkes, D.M., Semenza, G.L., Wirtz, D., 2014. Hypoxia and the extracellular matrix: drivers of tumour metastasis. Nat. Rev. Cancer 14, 430–439.

Hlatky, L., Hahnfeldt, P., Folkman, J., 2002. Clinical application of antiangiogenic therapy: microvessel density, what it does and doesn't tell us. J. Natl. Cancer Inst. 94, 883–893.

Hurwitz, H., Fehrenbacher, L., Novotny, W., Cartwright, T., Hainsworth, J., Heim, W., Berlin, J., Baron, A., Griffing, S., Holmgren, E., Ferrara, N., Fyfe, G., Rogers, B., Ross, R., Kabbinavar, F., 2004. Bevacizumab plus irinotecan, fluorouracil, and leucovorin for metastatic colorectal cancer. N. Engl. J. Med. 350, 2335–2342.

Huynh, H., Chow, P.K., Tai, W.M., Choo, S.P., Chung, A.Y., Ong, H.S., Soo, K.C., Ong, R., Linnartz, R., Shi, M.M., 2012. Dovitinib demonstrates antitumor and antimetastatic activities in xenograft models of hepatocellular carcinoma. J. Hepatol. 56, 595–601.

Jain, R., 2013a. Measurements of tumor vascular leakiness using DCE in brain tumors: clinical applications. NMR Biomed. 26, 1042–1049.

Jain, R.K., 2005. Normalization of tumor vasculature: an emerging concept in antiangiogenic therapy. Science 307, 58–62.

Jain, R.K., 2008. Lessons from multidisciplinary translational trials on anti-angiogenic therapy of cancer. Nat. Rev. Cancer 8, 309–316.

Jain, R.K., 2013b. Normalizing tumor microenvironment to treat cancer: bench to bedside to biomarkers. J. Clin. Oncol. 31, 2205–2218.

Kerbel, R.S., 2006. Antiangiogenic therapy: a universal chemosensitization strategy for cancer? Science 312, 1171–1175.

Kerbel, R.S., 2011. Reappraising antiangiogenic therapy for breast cancer. Breast 20 (Suppl. 3), S56–S60.

Kerbel, R.S., 2012. Strategies for improving the clinical benefit of antiangiogenic drug based therapies for breast cancer. J. Mammary Gland Biol. Neoplasia 17, 229–239.

Kerbel, R.S., Guerin, E., Francia, G., Xu, P., Lee, C.R., Ebos, J.M., Man, S., 2013. Preclinical recapitulation of antiangiogenic drug clinical efficacies using models of early or late stage breast cancer metastatis. Breast 22 (Suppl. 2), S57–S65.

Lawler, P.R., Lawler, J., 2012. Molecular basis for the regulation of angiogenesis by thrombospondin-1 and -2. Cold Spring Harb Perspect. Med. 2 a006627.

Lee, S.H., Lopes de Menezes, D., Vora, J., Harris, A., Ye, H., Nordahl, L., Garrett, E., Samara, E., Aukerman, S.L., Gelb, A.B., Heise, C., 2005. In vivo target modulation and biological activity of CHIR-258, a multitargeted growth factor receptor kinase inhibitor, in colon cancer models. Clin. Cancer Res. 11, 3633–3641.

Limaverde-Sousa, G., Sternberg, C., Ferreira, C.G., 2014. Antiangiogenesis beyond VEGF inhibition: a journey from

antiangiogenic single-target to broad-spectrum agents. Cancer Treat Rev. 40, 548–557.
Miller, K., Wang, M., Gralow, J., Dickler, M., Cobleigh, M., Perez, E.A., Shenkier, T., Cella, D., Davidson, N.E., 2007. Paclitaxel plus bevacizumab versus paclitaxel alone for metastatic breast cancer. N. Engl. J. Med. 357, 2666–2676.
Perren, T.J., Swart, A.M., Pfisterer, J., Ledermann, J.A., Pujade-Lauraine, E., Kristensen, G., Carey, M.S., Beale, P., Cervantes, A., Kurzeder, C., du Bois, A., Sehouli, J., Kimmig, R., Stahle, A., Collinson, F., Essapen, S., Gourley, C., Lortholary, A., Selle, F., Mirza, M.R., Leminen, A., Plante, M., Stark, D., Qian, W., Parmar, M.K., Oza, A.M., Investigators, I., 2011. A phase 3 trial of bevacizumab in ovarian cancer. N. Engl. J. Med. 365, 2484–2496.
Petrillo, M., Scambia, G., Ferrandina, G., 2012. Novel targets for VEGF-independent anti-angiogenic drugs. Expert Opin. Investig. Drugs 21, 451–472.
Richey, S.L., Hutson, T.E., 2013. Angiopoietins and non-vascular endothelial growth factor antiangiogenic targets in advanced renal cell carcinoma. Cancer J. 19, 307–310.
Rischin, D., Hicks, R.J., Fisher, R., Binns, D., Corry, J., Porceddu, S., Peters, L.J., 2006a. Prognostic significance of [18F]-misonidazole positron emission tomography-detected tumor hypoxia in patients with advanced head and neck cancer randomly assigned to chemoradiation with or without tirapazamine: a substudy of Trans-Tasman Radiation Oncology Group Study 98.02. J. Clin. Oncol. 24, 2098–2104.
Rischin, D., Hicks, R.J., Fisher, R., Binns, D., Corry, J., Porceddu, S., Peters, L.J.Trans-Tasman Radiation Oncology Group, S., 2006b. Prognostic significance of [18F]-misonidazole positron emission tomography-detected tumor hypoxia in patients with advanced head and neck cancer randomly assigned to chemoradiation with or without tirapazamine: a substudy of Trans-Tasman Radiation Oncology Group Study 98.02. J. Clin. Oncol. 24, 2098–2104.
Rolny, C., Mazzone, M., Tugues, S., Laoui, D., Johansson, I., Coulon, C., Squadrito, M.L., Segura, I., Li, X., Knevels, E., Costa, S., Vinckier, S., Dresselaer, T., Akerud, P., De Mol, M., Salomaki, H., Phillipson, M., Wyns, S., Larsson, E., Buysschaert, I., Botling, J., Himmelreich, U., Van Ginderachter, J.A., De Palma, M., Dewerchin, M., Claesson-Welsh, L., Carmeliet, P., 2011. HRG inhibits tumor growth and metastasis by inducing macrophage polarization and vessel normalization through downregulation of PlGF. Cancer Cell 19, 31–44.
Rubio-Viqueira, B., Jimeno, A., Cusatis, G., Zhang, X., Iacobuzio-Donahue, C., Karikari, C., Shi, C., Danenberg, K., Danenberg, P.V., Kuramochi, H., Tanaka, K., Singh, S., Salimi-Moosavi, H., Bouraoud, N., Amador, M.L., Altiok, S., Kulesza, P., Yeo, C., Messersmith, W., Eshleman, J., Hruban, R.H., Maitra, A., Hidalgo, M., 2006. An in vivo platform for translational drug development in pancreatic cancer. Clin. Cancer Res. 12, 4652–4661.
Sakurai, T., Kudo, M., 2011. Signaling pathways governing tumor angiogenesis. Oncology 81 (Suppl. 1), 24–29.
Sandler, A., Gray, R., Perry, M.C., Brahmer, J., Schiller, J.H., Dowlati, A., Lilenbaum, R., Johnson, D.H., 2006. Paclitaxel-carboplatin alone or with bevacizumab for non-small-cell lung cancer. N. Engl. J. Med. 355, 2542–2550.
Sharpless, N.E., Depinho, R.A., 2006. The mighty mouse: genetically engineered mouse models in cancer drug development. Nat. Rev. Drug Discov. 5, 741–754.
Van der Veldt, A.A., Lubberink, M., Bahce, I., Walraven, M., de Boer, M.P., Greuter, H.N., Hendrikse, N.H., Eriksson, J., Windhorst, A.D., Postmus, P.E., Verheul, H.M., Serne, E.H., Lammertsma, A.A., Smit, E.F., 2012. Rapid decrease in delivery of chemotherapy to tumors after anti-VEGF therapy: implications for scheduling of anti-angiogenic drugs. Cancer Cell 21, 82–91.
Wang, J., Foehrenbacher, A., Su, J., Patel, R., Hay, M.P., Hicks, K.O., Wilson, W.R., 2012. The 2-nitroimidazole EF5 is a biomarker for oxidoreductases that activate the bioreductive prodrug CEN-209 under hypoxia. Clin. Cancer Res. 18, 1684–1695.
Yan, M., Lesyk, G., Radziwon-Balicka, A., Jurasz, P., 2014. Pharmacological regulation of platelet factors that influence tumor angiogenesis. Semin. Oncol. 41, 370–377.
Yang, J.C., Haworth, L., Sherry, R.M., Hwu, P., Schwartzentruber, D.J., Topalian, S.L., Steinberg, S.M., Chen, H.X., Rosenberg, S.A., 2003. A randomized trial of bevacizumab, an anti-vascular endothelial growth factor antibody, for metastatic renal cancer. N. Engl. J. Med. 349, 427–434.